

Jet broadening in unstable non-Abelian plasmas

Adrian Dumitru,¹ Yasushi Nara,² Björn Schenke,¹ and Michael Strickland¹

¹*Institut für Theoretische Physik, Johann Wolfgang Goethe-Universität Frankfurt, Max-von-Laue-Straße 1, D-60438 Frankfurt am Main, Germany*

²*Akita International University, 193-2 Okutsubakidai, Yuwa-Tsubakigawa, Akita-City, Akita 010-1211, Japan*

(Received 15 October 2007; published 25 August 2008)

We perform numerical simulations of the SU(2) Boltzmann-Vlasov equation including both hard elastic particle collisions and soft interactions mediated by classical Yang-Mills fields. Using this technique we calculate the momentum-space broadening of high-energy jets in real time for both locally isotropic and anisotropic plasmas. In both cases we introduce a separation scale that separates hard and soft interactions and demonstrate that our results for jet broadening are independent of the precise separation scale chosen. For an isotropic plasma this allows us to calculate the jet transport coefficient \hat{q} including hard and soft nonequilibrium dynamics. For an anisotropic plasma the jet transport coefficient becomes a tensor with $\hat{q}_L \neq \hat{q}_\perp$. We find that for weakly coupled anisotropic plasmas the fields develop unstable modes, forming configurations where $B_\perp > E_\perp$ and $E_z > B_z$, which lead to $\hat{q}_L > \hat{q}_\perp$. We study whether the effect is strong enough to explain the experimental observation that high-energy jets traversing the plasma perpendicular to the beam axis experience much stronger broadening in rapidity, $\Delta\eta$, than in azimuth, $\Delta\phi$.

DOI: [10.1103/PhysRevC.78.024909](https://doi.org/10.1103/PhysRevC.78.024909)

PACS number(s): 12.38.Mh, 24.85.+p, 25.75.Dw, 25.75.Nq

I. INTRODUCTION

High transverse momentum jets produced in heavy-ion collisions represent a valuable tool for studies of the properties of the hot parton plasma produced in the central rapidity region [1]. This is due to the fact that jets couple to the plasma causing the jet to broaden in momentum space and to lose energy. The magnitude of momentum-space broadening and energy loss experienced by a parton depends on whether or not one assumes the matter to be hadronic or partonic in nature. Hence, it is one of the primary observables to ascertain experimentally whether or not the plasma has been produced. At very high energies it is expected that hard bremsstrahlung processes dominate the light quark or gluon energy loss [2]; however, at intermediate energies the inclusion of both collisional and radiative processes is necessary to make phenomenological predictions. Here we present the first results from real-time solution of the SU(2) Boltzmann-Vlasov equation for locally isotropic and anisotropic plasmas that include both hard (scattering) and soft (classical field) processes.

We first demonstrate that, in a locally isotropic plasma, one can obtain a cutoff independent transport coefficient \hat{q} , which measures the square of the transverse momentum transfer per mean free path. This measurement lays the groundwork for determining other jet transport properties like the energy-loss spectrum from real-time simulations. We then perform a similar measurement in a locally anisotropic plasma and demonstrate that for a non-Abelian plasma unstable modes can cause asymmetric broadening of jets. This may be relevant for recent measurements of dihadron correlations that provide evidence for an *asymmetric* broadening of jet profiles in the plane of pseudorapidity (η) and azimuthal angle (ϕ), with $\Delta\eta > \Delta\phi$, which has been called “the ridge” by experimentalists [1,3]. Here we show that this asymmetry could partly be caused by unstable plasma modes that are induced by the longitudinal expansion of the plasma.

At the earliest times after an ultrarelativistic heavy-ion collision, before thermalization and hydrodynamic expansion, the plasma undergoes rapid longitudinal expansion. This expansion can lead to an oblate anisotropic ($\langle p_z^2 \rangle \ll \langle p_\perp^2 \rangle$) momentum distribution in the local rest frame [4,5]. It has been shown that instabilities develop [5] in such anisotropic plasmas which lead to the formation of long-wavelength chromomagnetic and chromoelectric fields. These fields can then affect the propagation of hard jets and their induced hard radiation field. In the Abelian case soft transverse magnetic fields, B_\perp , dominate all other field components and therefore in this case one expects the longitudinal pressure induced by unstable modes to be larger than the transverse pressure [6,7]. This pressure asymmetry causes asymmetric broadening of jets with larger broadening along the longitudinal or η direction.

The situation is more complicated in non-Abelian plasmas because, in addition to generating large coherent B_\perp and E_\perp domains, one also generates large-amplitude longitudinal fields B_z and E_z . It is, therefore, not obvious a priori that the pressure generated by other field components will result in an asymmetric broadening of the jet. Through our numerical simulations we find that, for oblate parton momentum distributions, at different times either $E_z > B_z$ or $B_\perp > E_\perp$, with the net effect being a factor of 1.5 stronger longitudinal than transverse broadening.

II. BOLTZMANN-VLASOV EQUATION FOR NON-ABELIAN GAUGE THEORIES

We solve the classical transport equation for hard gluons with SU(2) color charge $q = q^a t^a$ [8], with the color generators t^a , including hard binary collisions

$$p^\mu [\partial_\mu + g q^a F_{\mu\nu}^a \partial_\nu + g f^{abc} A_\mu^b(x) q^c \partial_{q^a}] f = \mathcal{C}, \quad (1)$$

where $f = f(x, p, q)$ denotes the single-particle phase-space distribution. It is coupled self-consistently to the Yang-Mills equation for the soft gluon fields,

$$D_\mu F^{\mu\nu} = j^\nu = g \int \frac{d^3 p}{(2\pi)^3} dq q v^\nu f(x, p, q), \quad (2)$$

with $v^\mu = (1, \mathbf{p}/p)$. When the phase-space density is parametrically small, $f = \mathcal{O}(1)$, the collision term is given by

$$C = \frac{1}{4E_1} \int_{\mathbf{p}_2} \int_{\mathbf{p}'_1} \int_{\mathbf{p}'_2} (2\pi)^4 \delta^{(4)}(p'_1 + p'_2 - p_1 - p_2) \times (f'_1 f'_2 |\mathcal{M}_{1'2' \rightarrow 12}|^2 - f_1 f_2 |\mathcal{M}_{12 \rightarrow 1'2'}|^2), \quad (3)$$

with $\int_{\mathbf{p}_i} = \int \frac{d^3 p_i}{(2\pi)^3 2E_i}$. The matrix element \mathcal{M} includes all $gg \rightarrow gg$ tree-level diagrams and color factors as appropriate for the SU(2) gauge group.

We employ the test particle method to replace the continuous distribution $f(x, p, q)$ by a large number of test particles, which leads to Wong's equations [9]

$$\dot{\mathbf{x}}_i(t) = \mathbf{v}_i(t), \quad (4)$$

$$\dot{\mathbf{p}}_i(t) = g q_i^a(t) (\mathbf{E}^a(t) + \mathbf{v}_i(t) \times \mathbf{B}^a(t)), \quad (5)$$

$$\dot{q}_i(t) = -i g v_i^\mu(t) [A_\mu(t), q_i(t)], \quad (6)$$

for the i th test particle, whose coordinates are $\mathbf{x}_i(t)$, $\mathbf{p}_i(t)$, and $q_i^a(t)$. The time evolution of the Yang-Mills field is determined by the standard Hamiltonian method [10] in $A^0 = 0$ gauge. Our lattices have periodic boundary conditions and a lattice spacing a , the physical value of which is fixed by the length of the lattice $L = a N_s$. Dimensionless lattice variables scale such that when the number N_s of lattice sites is changed, L remains fixed (see Refs. [11,12] for details).

The theory without collisions as given by Eqs. (4)–(6) coupled to the lattice Yang-Mills equations was first solved in Ref. [13] to study Chern-Simons number diffusion in non-Abelian gauge theories at finite temperature. It was applied later also to the problem of gauge-field instabilities in anisotropic SU(2) plasmas [11,12]. Our numerical implementation is based on the improved formulation detailed in Ref. [12], where the non-Abelian currents generated by the hard particle modes on the lattice sites are “smeared” in time. This technique makes simulations in three dimensions on large lattices possible in practice.

In this article we go beyond those earlier simulations by accounting also for hard (short-distance) collisions among particles. The collision term is incorporated using the stochastic method [14]. Scattering processes are determined by sampling possible transitions according to the collision rate in a lattice cell:

$$\frac{dP_{2 \rightarrow 2}}{dt} = \tilde{v}_{\text{rel}} \frac{\sigma_{2 \rightarrow 2}}{a^3 N_{\text{test}}}, \quad (7)$$

with $\tilde{v}_{\text{rel}} = s/(2E_1 E_2)$, where s is the invariant mass of a gluon pair. The total cross section is given by

$$\sigma_{2 \rightarrow 2} = \int_{k^*}^{s/2} \frac{d\sigma}{dq^2} dq^2. \quad (8)$$

The momentum transfer is determined in the center of mass frame of the two colliding particles from the probability

distribution

$$\mathcal{P}(q^2) = \frac{1}{\sigma_{2 \rightarrow 2}} \frac{d\sigma}{dq^2}. \quad (9)$$

In Eq. (8) we have introduced an infrared cutoff k^* for point-like binary collisions. To avoid double-counting, this cutoff should be on the order of the hardest field mode that can be represented on the given lattice, $k^* \simeq \pi/a$. Momentum transfers below k^* are mediated by the classical Yang-Mills field; a soft scattering corresponds to deflection of a particle in the field of the other(s). Note that we use the color averaged expression for the collision term. The color charge of a particle is hence not affected by a hard collision.

Physically, the separation scale k^* should be sufficiently small so that the soft field modes below k^* are highly occupied [10]. On the other hand, k^* should be sufficiently large to ensure that hard modes can be represented by particles and that collisions are described correctly by Eq. (3). Furthermore, unstable modes arise in anisotropic plasmas (see below), all of which should be located below k^* . Because $g \sim 1$, in practice, we choose $k^* = \sqrt{3}\pi/a$ to be on the order of the temperature for isotropic systems and on the order of the hard transverse momentum scale for anisotropic plasmas. Independently, one should have $m_\infty L \gg 1$ and $m_\infty a \ll 1$: the first condition ensures that the relevant soft modes actually fit on the lattice while the latter corresponds to the continuum limit. Here, m_∞ denotes the soft scale and is given by

$$m_\infty^2 = g^2 N_c \int \frac{d^3 p}{(2\pi)^3} \frac{f(\mathbf{p})}{|\mathbf{p}|} \sim g^2 N_c \frac{n_g}{p_h}, \quad (10)$$

where $N_c = 2$ is the number of colors and n_g denotes the number density of hard gluons, summed over two helicities and $N_c^2 - 1$ colors. Also, $p_h \approx 3T$ is the typical momentum of a hard particle from the medium.

As we have argued above, we shall choose the inverse lattice spacing to be on the order of the temperature of the medium. Thus, with Eq. (10) the continuum condition $m_\infty a \ll 1$ roughly translates into

$$g^2 N_c \frac{n_g}{T^3} \ll 1. \quad (11)$$

To satisfy this relation with $g \sim 1$, in our numerical simulations below we shall assume an extremely hot medium, $T^3 \gg n_g$. However, this should be viewed simply as a numerical procedure, which ensures that the simulations are carried out near the continuum (or weak-coupling) limit. We verify below that transverse momentum broadening of a high-energy jet passing through a thermal medium is independent of T if the density and the ratio of jet momentum to temperature is fixed [compare to Eq. (13) below]. One may therefore obtain a useful “weak-coupling” estimate of $\langle p_\perp^2 \rangle$ (resp. for the related transport coefficient \hat{q}) by extrapolating our measurements down to realistic temperatures.

III. JET BROADENING IN AN ISOTROPIC PLASMA

We first consider a heat bath of particles with a density of $n_g = 10/\text{fm}^3$ and an average particle momentum of $3T = 12 \text{ GeV}$. The rather extreme “temperature” is chosen to satisfy

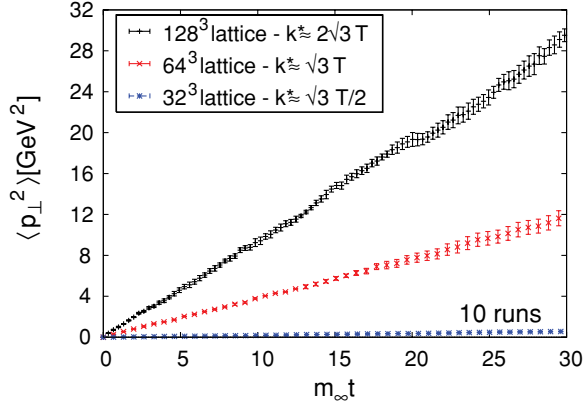


FIG. 1. (Color online) Momentum diffusion caused by particle-field interactions only. Additional high-momentum modes on larger lattices cause stronger momentum broadening. $T = 4$ GeV, $g = 2$, $N_c = 2$, $n_g = 10/\text{fm}^3$, $m_{\infty} = 1.4/\text{fm}$.

the above conditions on $N_s = 32 \dots 128$ lattices, assuming $L = 15$ fm. For a given lattice (resp. k^*) we take the initial energy density of the thermalized fields to be

$$\int \frac{d^3k}{(2\pi)^3} k \hat{f}_{\text{Bose}}(k) \Theta(k^* - k), \quad (12)$$

where $\hat{f}_{\text{Bose}}(k) = n_g / (2T^3 \zeta(3)) / (e^{k/T} - 1)$ is a Bose distribution normalized to the assumed particle density n_g and ζ is the Riemann ζ function. This is equivalent to the energy density of Bose-distributed particles with momenta below the separation momentum k^* . The initial spectrum is fixed to Coulomb gauge and $A_i \sim 1/k$ (in continuum notation); also, for simplicity we set $E_i = 0$ at the initial time but electric fields build up quickly within just a few time steps.

We then measure the momentum broadening $\langle p_{\perp}^2 \rangle(t)$ of high-energy test particles ($p/3T \approx 5$) passing through this medium. Figure 1 shows that in the collisionless case, $C = 0$, the broadening is stronger on larger lattices, which accommodate harder field modes. However, Fig. 2 demonstrates that collisions with momentum exchange larger than $k^*(a)$ compensate for this growth and lead to approximately lattice-

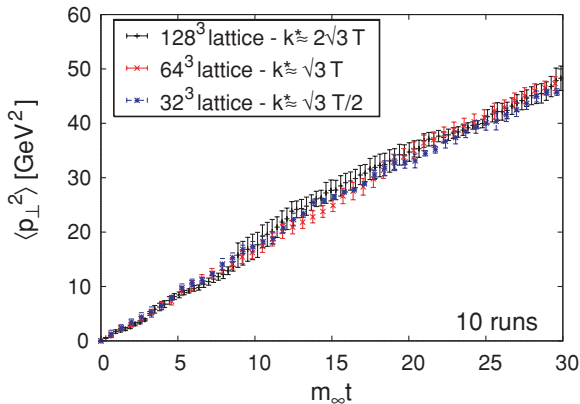


FIG. 2. (Color online) Momentum diffusion by both particle-field and direct particle-particle interactions. The result is independent of the separation scale k^* . Same parameters as in Fig. 1.

spacing independent results even when k^* varies by a factor of four.

Figures 1 and 2 show that the relative contributions to $\langle p_{\perp}^2 \rangle$ from soft and hard exchanges can depend significantly on k^* , even for $p/k^* = \mathcal{O}(10)$. It is clear, therefore, that transport coefficients obtained in the leading logarithmic (LL) approximation from the pure Boltzmann approach (without soft fields) will be rather sensitive to the infrared cutoff k^* . Fitting the difference of Fig. 2 and Fig. 1 (i.e., the hard contribution) to the LL formula,

$$\frac{d\langle p_{\perp}^2 \rangle}{dt} = \frac{C_A}{C_F} \frac{g^4}{8\pi} n_g \log\left(C^2 \frac{p^2}{k^{*2}}\right), \quad (13)$$

gives $C \simeq 0.43, 0.41, 0.31$ for $k^*/T = 2\sqrt{3}, \sqrt{3}, 0.5\sqrt{3}$, respectively. For the full calculation $C \simeq 0.61k^*/(\sqrt{3}T)$.

A related and frequently used transport coefficient is \hat{q} [2]. It is the typical momentum transfer (squared) per collision divided by the mean-free path, which is nothing but $\langle p_{\perp}^2 \rangle(t)/t$. From Fig. 2, $\hat{q} \simeq 2.2$ GeV²/fm for $N_c = 2$, $n_g = 10/\text{fm}^3$ and $p/(3T) \approx 5$. Our cutoff independent value for \hat{q} is in the range extracted from phenomenological analyses of jet-quenching data from BNL Relativistic Heavy Ion Collider (RHIC) [15].

In Fig. 3 we show that \hat{q} is indeed largely independent of the separation scale k^* . In these simulations, test particles were explicitly bunched into colorless jets, such that radiative energy loss does not contribute. This explains why one does not need bremsstrahlung processes in the collision term to obtain a cutoff independent result. Note that the magnitude of $\hat{q} \simeq 1.3$ GeV²/fm at $n_g = 5/\text{fm}^3$ and $p/(3T) = 16$ is smaller than the extrapolation obtained from Eq. (13) with the constant under the logarithm fixed from the previous runs at $n_g = 10/\text{fm}^3$ and $p/(3T) = 5$; hence, C effectively depends on the density and the jet momentum.

In Fig. 4 we verify that \hat{q} does not depend on the temperature T so long as the particle density n_g and the ratio of jet momentum to temperature, p/T , is fixed. Thus, our measurement of $\hat{q} \simeq 2.2$ GeV²/fm may be considered as a weak-coupling extrapolation to realistic temperatures of $T \approx 300$ MeV and jet momenta of about 4.5 GeV.

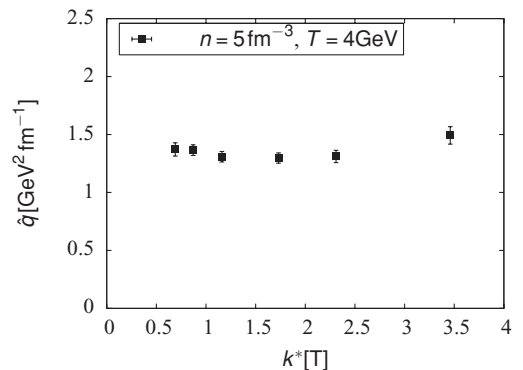
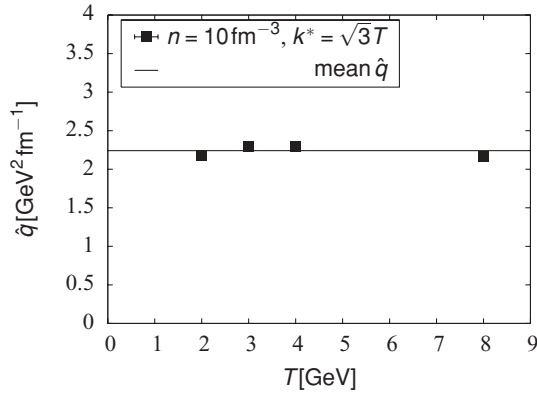


FIG. 3. \hat{q} as a function of k^* at fixed $n_g = 5/\text{fm}^3$ and $p/(3T) = 16$.


 FIG. 4. \hat{q} as a function of T at fixed $n_g = 10/\text{fm}^3$ and $p/(3T) = 5$.

IV. JET BROADENING IN AN UNSTABLE PLASMA

In heavy-ion collisions, locally anisotropic momentum distributions can emerge due to the longitudinal expansion. Such anisotropies generically give rise to instabilities [5]; see Refs. [11,12] for simulations of unstable non-Abelian plasmas within the present ‘‘Wong-Yang-Mills’’ approach. Here, we investigate their effect on the momentum broadening of jets, including the effect of collisions. The initial momentum distribution for the hard plasma gluons is taken to be

$$f(\mathbf{p}) = n_g \left(\frac{2\pi}{p_h} \right)^2 \delta(p_z) \exp(-p_\perp/p_h), \quad (14)$$

with $p_\perp = \sqrt{p_x^2 + p_y^2}$. This represents a quasithermal distribution in two dimensions with average momentum $= 2 p_h$. We initialize small-amplitude fields sampled from a Gaussian distribution and set $k^* \approx p_h$, for the reasons alluded to above. The band of unstable modes is located below k^* .

We find that binary collisions among hard particles reduce the growth rate of unstable field modes, in agreement with expectations [16]. However, for $p_h = 16 \text{ GeV}$, $L = 5 \text{ fm}$, $n_g = 10/\text{fm}^3$, $g = 2$, $m_\infty \simeq 1/\text{fm}$, and $k^* \approx 1.7 p_h$, the reduction of the growth rate is only approximately 5%, increasing to about 15% when $k^* \approx 0.9 p_h$. This is due to fewer available field modes and more randomizing collisions.

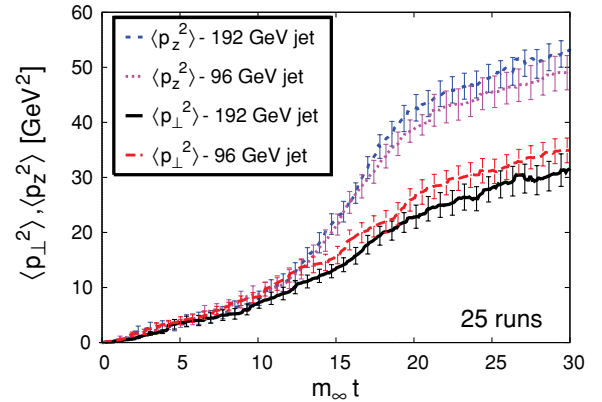
Next, we add additional high-momentum particles with $p_x = 12 p_h$ and $p_x = 6 p_h$, respectively, to investigate the broadening in the y and z directions via the variances

$$\hat{q}_\perp(p_x) := \frac{d}{dt} \langle (\Delta p_\perp)^2 \rangle, \quad \hat{q}_L(p_x) := \frac{d}{dt} \langle (\Delta p_z)^2 \rangle. \quad (15)$$

The quantity $\sqrt{\hat{q}_L/\hat{q}_\perp}$ can be roughly associated with the ratio of jet correlation widths in azimuth and rapidity: $\sqrt{\hat{q}_L/\hat{q}_\perp} \approx \langle \Delta \eta \rangle / \langle \Delta \phi \rangle$.

Figure 5 shows the time evolution of $\langle p_\perp^2 \rangle$ and of $\langle p_z^2 \rangle$. The strong growth of the soft fields sets in at about $t \simeq 10 m_\infty^{-1}$ and saturates around $t \simeq 25 m_\infty^{-1}$ due to the finite lattice spacing (also see Ref. [12]). Outside the above time interval the ratio $\hat{q}_L/\hat{q}_\perp \approx 1$. During the period of instability, however,

$$\frac{\hat{q}_L}{\hat{q}_\perp} \approx 2.3, \quad (16)$$

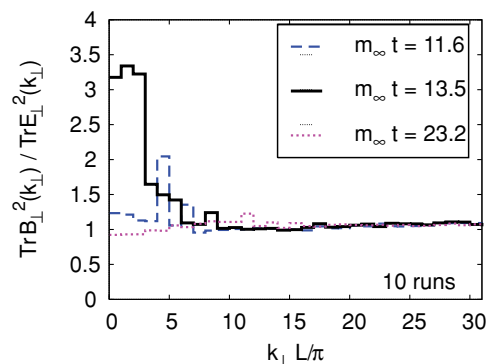

 FIG. 5. (Color online) Momentum broadening of a jet in the directions transverse to its initial momentum. p_z is directed along the beam axis; p_\perp is transverse to the beam. Anisotropic plasma, 64^3 lattice.

for both jet energies shown in Fig. 5. We find approximately the same ratio for denser plasmas ($n_g = 20/\text{fm}^3$ and $n_g = 40/\text{fm}^3$). Reducing the number of lattice sites and scaling p_h down to 8 GeV gives $\hat{q}_L/\hat{q}_\perp \approx 2.1$. However, these latter runs are rather far from the continuum limit and lattice artifacts are significant [12].

The explanation for the larger broadening along the beam axis is as follows. In the Abelian case the instability generates predominantly transverse magnetic fields that deflect the particles in the z direction [7].

In the non-Abelian case, however, on three-dimensional lattices transverse magnetic fields are much less dominant (see, e.g., Fig. 5 in Ref. [12]) although they do form larger coherent domains in the transverse plane at intermediate times than E_\perp (Fig. 6). Longitudinal fields and locally nonzero Chern-Simons number $\sim \text{tr} \mathbf{E} \cdot \mathbf{B}$ emerge, also. Nevertheless, Fig. 7 shows that $E_z > B_z$, aside from $B_\perp > E_\perp$. Hence, the field configurations are such that particles are deflected preferentially in the longitudinal z direction (to restore isotropy).

A third contribution to p_z broadening in an expanding plasma, not considered explicitly here, is due to a longitudinal collective flow field that ‘‘blows’’ the jet fragments to the


 FIG. 6. (Color online) Ratios of Fourier transforms of the field energy densities (integrated over k_z) at various times; the gauge potentials were transformed to Coulomb gauge.

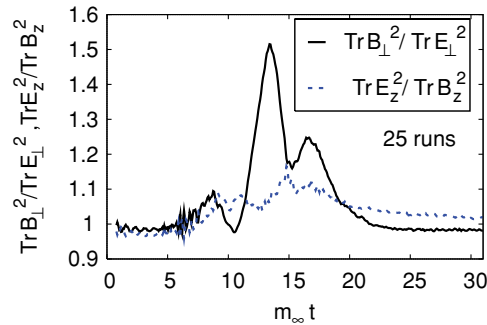


FIG. 7. (Color online) Ratios of field energy densities.

side [17]. This mechanism is also available for collision dominated plasmas with (nearly) isotropic momentum distribution. However, rather strong flow gradients seem to be required to reproduce the observed broadening of midrapidity jets (the flow velocity has to vary substantially *within* the narrow jet cone).

In contrast, color fields will naturally deflect particles with lower momentum by larger angles ($\Delta p \sim E, B$): the jet profile broadens even if the induced radiation is exactly collinear. It is therefore important to determine, experimentally, whether the asymmetric broadening is related to the *macroscopic* collective flow or to an anisotropy of the plasma in the local rest frame. More detailed simulations should account, also, for the fact that small- x gluons are already correlated over large rapidity intervals at the initial time [18].

ACKNOWLEDGMENTS

B.S. thanks O. Fochler, P. Romatschke, and Z. Xu for many useful discussions. The simulations were performed at the Center for Scientific Computing of Goethe University. B.S. also thanks the Institute for Nuclear Theory at the University of Washington for its hospitality. M.S. and B.S. are supported by DFG Grant GR 1536/6-1.

-
- [1] P. Jacobs, Eur. Phys. J. C **43**, 467 (2005).
 [2] R. Baier, Y. L. Dokshitzer, A. H. Mueller, S. Peigne, and D. Schiff, Nucl. Phys. **B484**, 265 (1997).
 [3] F. Wang (STAR Collaboration), J. Phys. G **30**, S1299 (2004); J. Adams *et al.* (STAR Collaboration), Phys. Rev. Lett. **95**, 152301 (2005); Phys. Rev. C **73**, 064907 (2006); J. Putschke, J. Phys. G **34**, S679 (2007).
 [4] R. Baier, A. H. Mueller, D. Schiff, and D. T. Son, Phys. Lett. **B502**, 51 (2001).
 [5] P. Romatschke and M. Strickland, Phys. Rev. D **68**, 036004 (2003); P. Arnold, J. Lenaghan, and G. D. Moore, J. High Energy Phys. **08** (2003) 002; S. Mrowczynski, Acta Phys. Pol. B **37**, 427 (2006).
 [6] P. Romatschke, Phys. Rev. C **75**, 014901 (2007); P. Romatschke and M. Strickland, Phys. Rev. D **71**, 125008 (2005).
 [7] A. Majumder, B. Müller, and S. A. Bass, Phys. Rev. Lett. **99**, 042301 (2007).
 [8] U. W. Heinz, Phys. Rev. Lett. **51**, 351 (1983); Ann. Phys. **161**, 48 (1985); **168**, 148 (1986); H.-T. Elze and U. W. Heinz, Phys. Rep. **183**, 81 (1989); J. P. Blaizot and E. Iancu, Phys. Rev. Lett. **70**, 3376 (1993); Nucl. Phys. **B417**, 608 (1994); P. F. Kelly, Q. Liu, C. Lucchesi, and C. Manuel, Phys. Rev. Lett. **72**, 3461 (1994); Phys. Rev. D **50**, 4209 (1994); D. F. Litim and C. Manuel, Phys. Rev. Lett. **82**, 4981 (1999); P. Arnold, G. D. Moore, and L. G. Yaffe, J. High Energy Phys. **01** (2003) 030.
 [9] S. K. Wong, Nuovo Cimento A **65**, 689 (1970).
 [10] J. Ambjorn, T. Askgaard, H. Porter, and M. E. Shaposhnikov, Nucl. Phys. **B353**, 346 (1991); A. Krasnitz and R. Venugopalan, *ibid.* **B557**, 237 (1999).
 [11] A. Dumitru and Y. Nara, Phys. Lett. **B621**, 89 (2005).
 [12] A. Dumitru, Y. Nara, and M. Strickland, Phys. Rev. D **75**, 025016 (2007).
 [13] C. R. Hu and B. Müller, Phys. Lett. **B409**, 377 (1997); G. D. Moore, C. Hu, and B. Müller, Phys. Rev. D **58**, 045001 (1998).
 [14] P. Danielewicz and G. F. Bertsch, Nucl. Phys. **A533**, 712 (1991); A. Lang, H. Babovsky, W. Cassing, U. Mosel, H. Reusch, and K. Weber, J. Comp. Physiol. **106**, 391 (1993); Z. Xu and C. Greiner, Phys. Rev. C **71**, 064901 (2005).
 [15] A. Majumder, J. Phys. G **34**, S377 (2007).
 [16] B. Schenke, M. Strickland, C. Greiner, and M. H. Thoma, Phys. Rev. D **73**, 125004 (2006).
 [17] N. Armesto, C. A. Salgado, and U. A. Wiedemann, Phys. Rev. C **72**, 064910 (2005).
 [18] A. Dumitru, F. Gelis, L. McLerran, and R. Venugopalan, arXiv:hep-ph/0804.3858.